Conditions of pluton emplacement and anatexis in the Caledonian Bindal Batholith, north-central Norway

CALVIN G. BARNES & TORE PRESTVIK

Barnes, C. G. & Prestvik, T.: Conditions of pluton emplacement and anatexis in the Caledonian Bindal Batholith, north-central Norway. *Norsk Geologisk Tidsskrift,* Vol. 80, pp. 259–274. Oslo 2000. ISSN 0029-196X.

The Velfjord plutons are mafic-intermediate plutons in the Bindal Batholith that were emplaced into pelitic and calcareous rocks of the Helgeland Nappe Complex of the Uppermost Allochthon at ~448 Ma. Al-in-hornblende barometry suggests emplacement in the range of 6 to 8 kbar, which is consistent wit the presence of magmatic epidote. Pelitic rocks in the aureoles underwent partial melting and leucosomes locally accumulated adjacent to the plutons to form "contact granites". The results of garnet-aluminosilicate-silica-plagioclase (GASP) thermobarometry combined with a recently published petrogenetic grid for dehydration partial melting of pelites suggest a clockwise P-T-t path for the wall rocks. The GASP results, plus the presence of early kyanite, suggest initial melting in the 7 to 8 kbar range. Temperatures close to the plutons reached at least 750°C to 800°C. Nearly isothermal decompression to ~4 to 5 kbar resulted in the hottest wall rocks reaching cordierite stability while they were still partly molten. Cooler wall rocks could not reach conditions of cordierite stability because of the positive slope of the cordierite-in equilibrium. The state of HNC crust prior to pluton emplacement cannot yet be determined. However, rapid exhumation of the plutons and their wall rocks suggests that the youngest plutons of t e Bindal Batholith were probably emplaced at lower pressures.

Calvin G. Barnes, Department of Geosciences, Texas Tech University, Lubbock, TX 79409-053, USA; Tore Prestvik, Department of Geology and Mineral Resources Engineering, Norwegian University of Science and Technology, Høgskoleringen 6, N-7491 Trondheim, Norway

Introduction

The Bindal Batholith is the largest Caledonian-age batholith in Norway (Fig. 1). It consists of dozens of plutons emplaced into the Helgeland Nappe Complex (HNC) from about 481 Ma to 430 Ma (Nordgulen et al. 1993; Pedersen et al. 1999). The Batholith contains a remarkably wide variety of rock types and compositions, from gabbro to granite (Nordgulen 1993). Elemental data (Nordgulen 1993; Barnes et al. 1992) and isotopic studies (Nordgulen & Sundvoll 1992; Birkeland et al. 1993) indicate that many of the plutons are either the products of crustal melting or that they contain a significant crustal component. Therefore, an understanding of the origin of the Batholith, and the evolution of the HNC, requires knowledge of the style and conditions of crustal melting during Caledonian time. In Velfjord, heat from mafic to intermediate plutons caused partial melting of their metapelitic wall rocks at about 448 Ma. Detailed study of these rocks can provide knowledge of melting reactions, the effect of deformation on melt extraction, and heat transfer in the crust. To that end, this paper presents the results of thermobarometric studies of pluton emplacement. The results suggest that the Velfjord plutons were emplaced during a clockwise P-T path and that exhumation followed while some of the wall rocks were still partly molten.

Geologic setting

The Bindal Batholith (Fig. 1) is the northernmost of two Ordovician-Silurian batholiths in north-central Norway; the other is the Smøla-Hitra Batholith west of Trondheim (Gautneb & Roberts 1989). The host rocks of the Batholith are part of the Helgeland Nappe Complex (HNC, Fig. 2) (Barnes et al. 1992; Gustavson 1978; Kollung 1967; Myrland 1972; Thorsnes & Løseth 1991), which is the structurally highest unit of the Uppermost Allochthon. The nappe is composite and consists of Late Proterozoic (Trønnes 1994), medium-to high-grade pelitic, semi-pelitic, calc-silicate, and calcareous rocks, and Early Ordovician ophiolite complexes along with their unconformable cover sequences of medium-to low-grade schists, metasandstones, metaconglomerates, and calc-silicate rocks (Thorsnes & Løseth 1991). Amalgamation of these units in the Velfjord area took place prior to emplacement of the Andalshatten pluton at about 448 Ma (Nordgulen et al. 1992; Ø. Nordgulen, pers. comm.) and therefore prior to intrusion of the coeval Velfjord plutons (see below). Eastward translation of the HNC, including the Bindal Batholith, across low-grade rocks of the Upper Allochthon took place in the Late Silurian to Devonian Scandian phase of the Caledonian orogeny (e.g. Stephens et al. 1985).

Plutonic rocks in the Bindal Batholith range from gabbro to granite, with intermediate to felsic calc-alkaline and alkali-calcic compositions most common. Although most plutons can be classified as I-type (Nordgulen 1993), reconnaissance Pb, Sr, and Nd isotopic studies indicate the presence of metasedimentary and meta-igneous crustal sources and a mantle component.

The large Velfjord plutons are, from north to south, Hillstadfjellet, Akset-Drevli, and Sausfjellet (Fig. 2, Barnes et al. 1992). The Sausfjellet pluton is predominantly dioritic whereas the Akset-Drevli pluton is Fe-rich

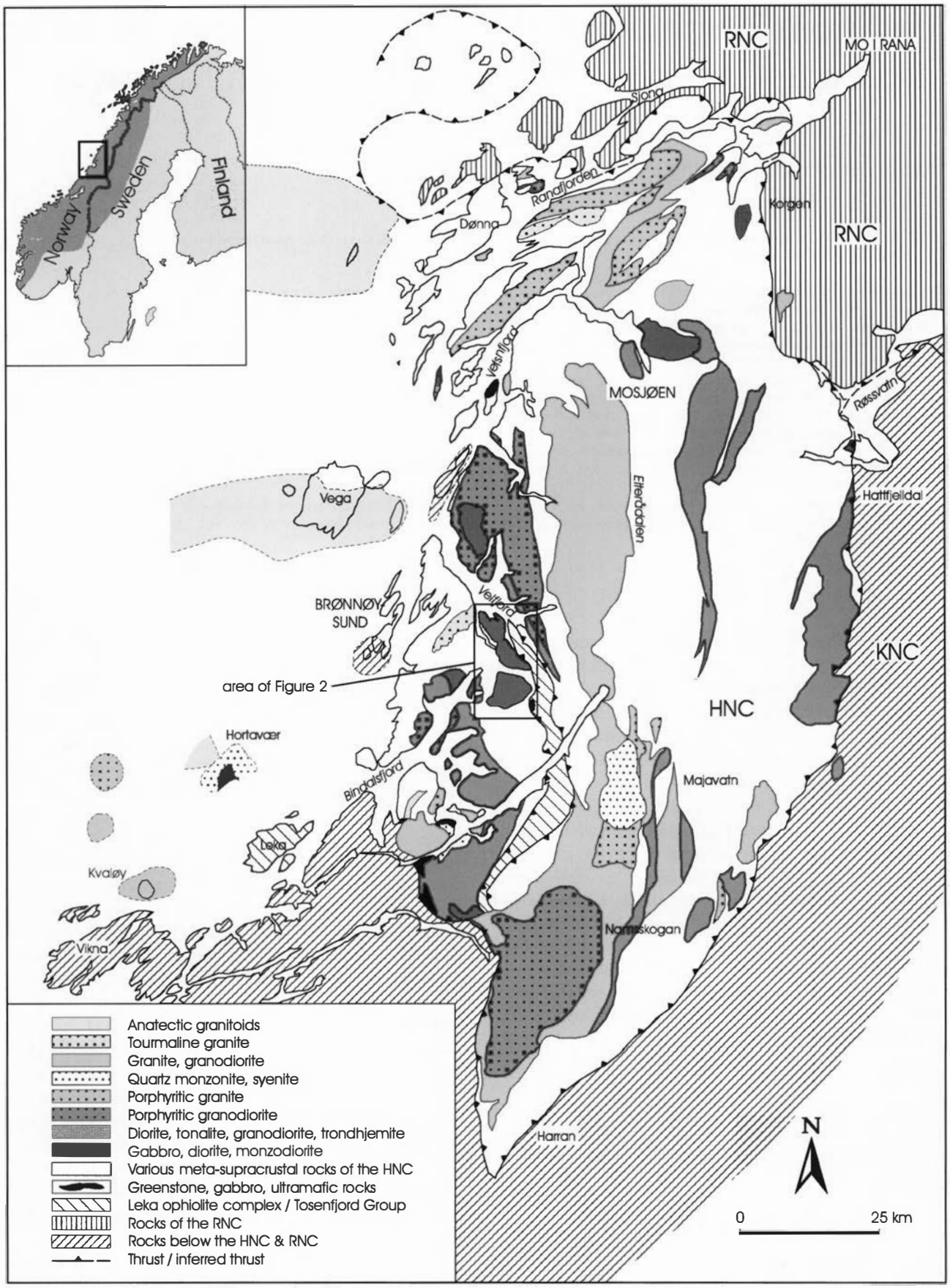

Fig. 1. Regional geologic setting of the Bindal Batholith. HNC, Helgeland Nappe Complex; RNC, Rödingsfjället Nappe Complex; KNC, Köli Nappe Complex.

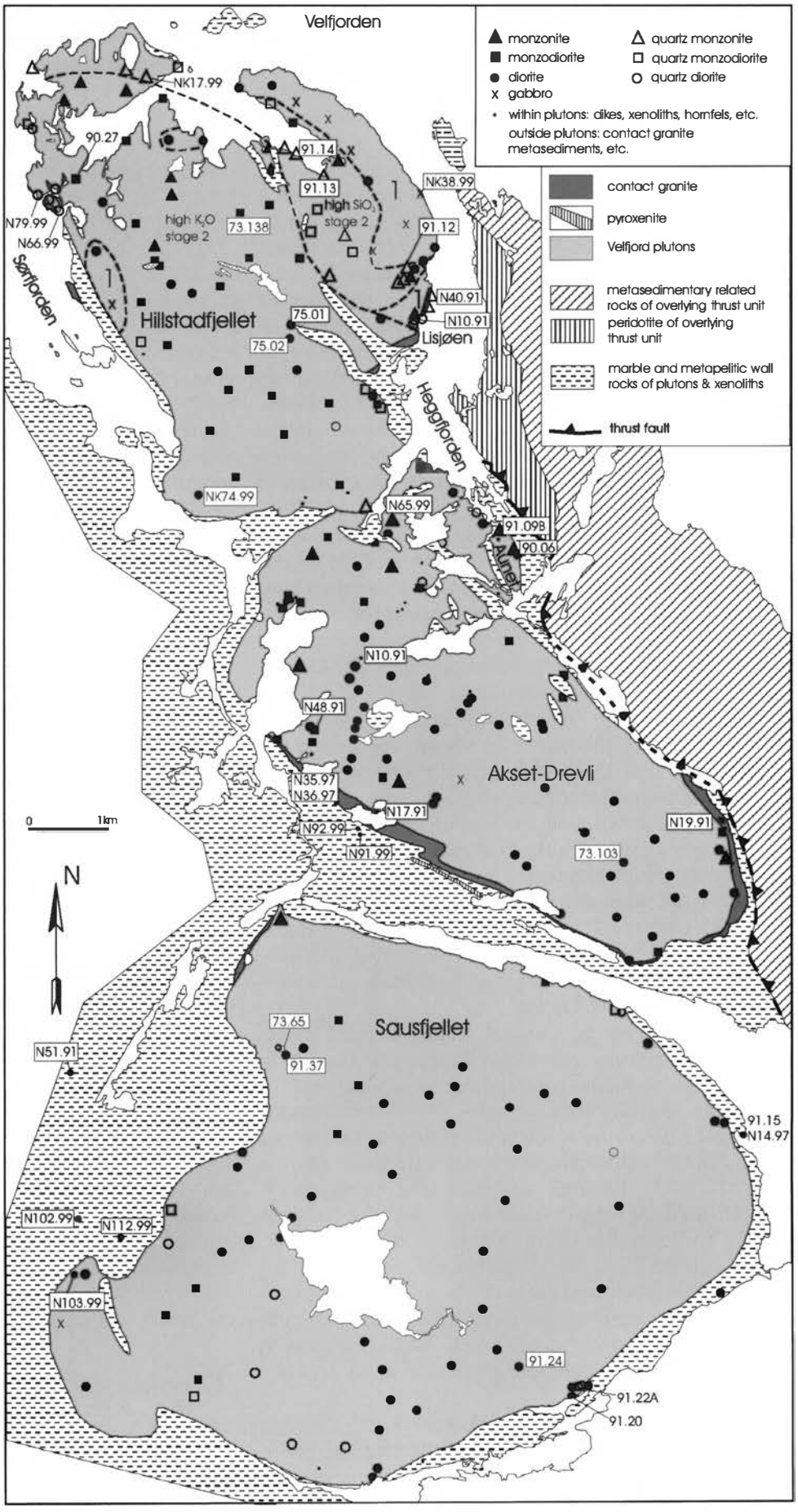

Fig. 2. Simplified geologic map of the Velfjord plutons, showing locations of analyzed samples.

diorite and gabbro (Fig. 2). A 1-km-long body of olivine pyroxenite that crops out south of the Akset-Drevli pluton is considered to be part of that plutonic sequence. The Hillstadfjellet pluton was emplaced in two stages: an early gabbroic Stage 1 and a later, more voluminous, monzonitic Stage 2 (Fig. 2).

The small monzonitic Aunet pluton underlies an area north of the Akset-Drevli pluton (Fig. 2) and crosscuts a sequence of gabbroic and dioritic dikes from that pluton and from Stage 1 of the Hillstadfjellet pluton. The Aunet monzonite is compositionally similar to Stage 2 of the Hillstadfjellet pluton (Barnes et al. 1992). Other small mafic bodies crop out southeast of Sausfjellet and west of Sørfjord (Myrland 1972; Thorsnes & Løseth 1991).

U-Pb ages on zircon fractions from the Velfjord plutons yield ages of 447 Ma and 448 Ma (Pedersen et al. 1999). These ages are comparable with other U-Pb ages from the batholith, which range from 447 Ma to 430 Ma (Nordgulen & Schouenborg 1990; Nordgulen et al. 1993). In addition to this Scandian activity, new U-Pb ages of granites from the Velfjord area are as old as 481 Ma (Pedersen et al. 1999), which indicates that granitic magmatism in the Bindal Batholith lasted longer and was more complex than originally thought. Furthermore, two fractions of elongate, prismatic zircons from a porphyritic granite adjacent to the southeastern side of the Hillstadfjellet pluton near Lisjøen (Fig. 2) yielded a concordant zircon age of 475 ± 3 Ma (Pedersen et al. 1999). Whether this age indicates the age of emplacement of the granite or whether the zircons are inherited is a topic that will be partially addressed in this paper and is the subject of on-going ion probe analysis.

At the level of exposure, the host rocks of the Velfjord plutons consist entirely of the high-grade Late Proterozoic unit (Fig. 2). Pelitic lithologies in this unit are commonly migmatitic, but some quartz-rich lithologies lack evidence of partial melting. The age of the (apparent) regional migmatization event has been thought to predate emplacement of the Velfjord plutons, but its precise age awaits detailed geochronological data.

Contacts between the Velfjord plutons and calcareous wall rocks are sharp and locally brecciated, but where pelitic gneisses would normally be in contact with a pluton, the contact zone consists of kilometer-length sections of a distinctive assemblage of porphyritic granitic rocks, diatexite (disrupted migmatite that lacks internal structure), and stromatic migmatite (Fig. 2). Contacts between these distinctive assemblages and the Velfjord plutons are generally sharp. Dikes of the porphyritic granite cut the Akset-Drevli pluton and Stage 1 of the Hillstadfjellet pluton and decimeter-scale dikes of diatexite intrude the margins of the Hillstadfjellet and Sausfjellet plutons. The porphyritic granitic rocks range from granite to tonalite, but they are herein referred to as 'contact granites'.

The degree of migmatization decreases with distance from plutonic contacts. Adjacent to the plutons, either contact granite or highly disrupted diatexite is typical. These rocks grade into zones in which pelitic compositions are diatexitic and more siliceous rocks are stromatic migmatite. Further from contacts, pelitic migmatites are stromatic and siliceous rocks are unmigmatized or are vein migmatite. These distinct types of migmatite occupy layers within the wall rock sequence. These field relationships suggest that the contact granites resulted from *in situ* anatexis of pelitic wall rocks. The heat necessary to form the contact granites was apparently supplied by the mafic Velfjord magmas.

As the plutonic contacts are approached and the proportion of leucosome in the wall rocks increases, migmatitic veins and dikes more commonly crosscut compositional layers. The leucosomes range from granitic to tonalitic in composition and most are equigranular. However, a few leucosomes contain K-feldspar megacrysts (up to 2 cm long), with textures similar to those of the porphyritic contact granites. Where crosscutting relationships were observed, the K-feldspar-phyric leucosomes are foliated and pinch out along strike of the foliation. These pinch-outs are tapered, not boundinaged, which suggests entrapment of the granitic magma during deformation. They are crosscut by later leucogranitic dikes.

Petrography

Plutonic rocks

Petrographic descriptions of the Velfjord plutons were presented in Barnes et al. (1992) and the mineral assemblages of analyzed samples are presented in Table 1. For the purposes of this account, amphibole petrography is particularly important. Amphibole varies in habit; it occurs as a rimming phase on pyroxene, as distinct prismatic to intergranular crystals, and as dispersed scrappy grains in granites. It is locally rimmed by biotite. In many samples, amphibole is color zoned, with olive green cores and blue-green rims. The width of these rims is variable, from a few microns to several tenths of a millimeter. In many evolved rocks, amphibole is entirely blue-green.

In addition to amphibole, many samples contain accessory epidote (Table 1), which occurs in two types. The first is as euhedral to subhedral weakly pleochroic (yellow) grains with allanite cores. These crystals are typically intergrown with biotite ± amphibole ± ilmenite. They commonly have euhedral faces against biotite and anhedral surfaces against plagioclase and quartz. The second type of epidote forms clear, equant to elongate, prismatic inclusions in plagioclase. Such inclusions are most common in plagioclase cores. In a few samples, the latter type of epidote occurs in plagioclase cores, whereas the former type is present as inclusions in plagioclase rims.

Migmatitic rocks

Stromatic migmatites are medium grained gneisses banded on a cm scale. They typically contain sillimanite, muscovite, biotite, quartz, and plagioclase ± garnet ± staurolite ± K-feldspar. Robust sillimanite prisms are sparse and

Table 1. Petrographic summary of analyzed samples.

Setting	Rock type and [essential minerals] {relict minerals}	Range of plag. An%	Accessory minerals
	Sausfjellet pluton		
73.65	Epidote amphibole biotite diorite	43–40	Qtz, Ttn, Zrn, Ilm, Ap
91.22A	Amphibole epidote biotite quartz diorite	34–27	Ttn, Zrn, Ap
91.24	Pyroxene amphibole diorite	71–57	Ttn, Ap
91.37	Amphibole epidote biotite granite	57–21	Aln, Ilm, Ap, Zrn, Ttn?
	Akset-Drevli pluton		
73.103	Olivine orthopyroxene augite diorite	42–37	Biotite, Ilm, Mt, Ap
N10.91	Hornblende orthopyroxene gabbro	71–63	Ap, Ilm, Mt
N48.91	Augite orthopyroxene monzodiorite	54–32	Ap, Ilm, Mt Olivine
	Hillstadfjellet pluton, Stage 1		
75.01	Pyroxene amphibole biotite gabbro	52–39	Ap, Ilm, Cal
75.02	Amphibole biotite quartz monzodiorite	36–14	Ap, Ilm, Ttn
NK38.99	Biotite amphibole gabbro	69–32	Ep, Ilm, Ap, Ttn
NK74.99	Biotite amphibole quartz gabbro	54–19	Ap, Ilm, Ttn
	Hillstadfjellet pluton, Stage 2		
73.138	Epidote-bearing amphibole biotite monzodiorite	47–14	Ep, Ilm, Ttn, Ap, Tur
90.27	Amphibole biotite monzodiorite	38–25	Ap, Ilm
91.12	Biotite amphibole quartz monzonite	42–14	Ep, Ttn, Aln, Zrc, Tur
91.13	Biotite amphibole quartz monzonite	50–14	Ap, Zrn, Ttn, Ilm, Tur
91.14	Biotite amphibole quartz monzonite	35–20	Ap, Zrn, Ttn, Ilm
NK17.99	Pyroxene amphibole biotite monzodiorite	77–25	Ilm, Ap
	Hillstadfjellet pluton, Stage 2 in contact zones		
N40.91	Amphibole epidote biotite quartz monzonite	49–12	Aln, Ep, Ilm, Ttn, Ap
N66.99	Amphibole biotite quartz monzodiorite	39–21	Ep, Ilm, Ap, Ttn
N79.99A	Epidote biotite amphibole quartz monzodiorite	58–29	Ap, Ilm, Zrn, Aln, Ccp
	Mingled rocks in Hillstadfjellet pluton contact zone		
91.10A	Garnet-bearing biotite hornblende tonalite	60–32	Ap, Ilm, Zrn
91.10B	Garnet-bearing biotite hornblende quartz diorite	nd	Ap
	Aunet pluton		
90.06	Pyroxene-bearing biotite amphibole quartz monzonite	26–17	Ttn, Ilm, Ap, Ep, Zrn, Cal
91.09B	Pyroxene amphibole monzonite	22–20	Ttn, Bi, Qtz, Zrn, Ilm
N65.99	Amphibole biotite cpx quartz monzonite	47–19	Ilm, Ap, Zrn
	Migmatitic wall rocks		
91.15A	{Cordierite} kyanite sillimanite garnet biotite diatexite [muscovite, K-feldspar, plagioclase, quartz]	87–52	Ilm, Zrn/Mnz
N51.91B	Staurolite garnet sillimanite muscovite biotite gneiss [plagioclase, quartz, K-feldspar]	nd	Ilm, Zrn/Mnz
N14.97A	Cordierite kyanite sillimanite garnet biotite diatexite [K-feldspar, plagioclase, quartz]	45–23	Ilm, Tur, St
N35.97	Sillimanite garnet biotite leucogranodiorite migmatitic leucosome	35–22	Ms, Ilm, Zrn
N36.97	Sillimanite garnet biotite diatexitic tonalitic gneiss	35–18	Ilm, Zrn/Mnz, St, Crd
N91.99	Muscovite sillimanite biotite garnet restite-rich dike [plagioclase, quartz]	37–29	Ilm, Ccp, Zrn, Crd
N92.99A	Sillimanite garnet biotite quartz dioritic diatexite	42–37	Ky
N102.99	Sillimanite garnet biotite granitic migmatitic gneiss	34–12	Ilm, Zrn/Mnz, Tur
N103.99	Sillimanite garnet biotite diatexitic diorite restite-rich dike	37–12	Qtz, St, Ilm, Tur, Zrn/Mnz
N112.99A	Sillimanite garnet muscovite biotite melagranitic gneiss	34–23	
	Contact granites		
N17.91	Garnet biotite opx tonalite	34–32	Kfs, Zrn, Ilm, Spl
N19.91	Sillimanite garnet muscovite biotite granite	46–27	Ap, Ilm, Zrn/Mnz

some are partly replaced by muscovite. Acicular to granular sillimanite is more common; it occurs along crystal boundaries and as inclusions in muscovite. Staurolite and garnet are euhedral against micas and ragged where in contact with quartz and plagioclase. Muscovite typically replaces sillimanite and is intergrown with biotite. In the latter case, it commonly crosscuts foliation formed by the biotite.

Diatexitic migmatites are medium grained and contain the assemblage plagioclase + quartz + biotite + sillimanite ± K-feldspar (microcline) ± kyanite ± cordierite ± muscovite. Foliation is generally weak and is defined by discontinuous banding, with or without orientation of biotite and sillimanite. A 'matrix' of quartz, granular to interstitial plagioclase, sparse poikilitic K-feldspar, biotite, and sillimanite surrounds porphyroblasts of garnet and cm-scale sillimanite. Quartz is generally interstitial to subpoikilitic.

Sillimanite is present in four habits: as sparse, stubby, cm-scale grains, as mm-scale elongate prisms, as acicular inclusions in other silicates (particularly biotite), and less commonly as fibrolitic mats. The coarse sillimanite crystals typically show deformation-induced subgrain development. Prismatic sillimanite is generally subparallel to banding or foliation and is locally bent or broken. Acicular sillimanite is generally unoriented, undeformed, and intergrown with biotite. Where present, kyanite occurs as ragged crystals, typically surrounded by biotite and quartz ± sillimanite. Some kyanite occurs as inclusions in cordierite.

Where cordierite is present, it varies from 4-mm long blocky crystals to ~0.5 mm diameter intergranular grains mostly enclosed in quartz (± sillimanite ± plagioclase). In all cases, cordierite is present in the leucocratic parts of the rock rather than in biotite-and garnet-rich zones. The cordierite is locally replaced by acicular sillimanite + pale biotite.

Garnet is poikiloblastic; its cores contain inclusions of quartz ± biotite ± sillimanite. Garnet rims are typically free of inclusions except for local concentrations of acicular sillimanite. Many crystals appear to be resorbed, whereas others have idiomorphic outlines. Individual crystals commonly show both of these features.

Reddish brown biotite rims and replaces cordierite and is intergrown with acicular and prismatic sillimanite. Much of the intergrown biotite and sillimanite are interstitial. Where muscovite is present, it replaces feldspars or forms discrete grains that crosscut the gneissic banding.

Anhedral ilmenite, tourmaline, zircon, monazite, apatite, chalcopyrite, and staurolite are accessories. The staurolite locally occurs as ragged mm-scale crystals. It is more common as fine euhedral prisms associated with intergranular biotite.

No petrographic break between regional and contact migmatites was observed. With approach to the plutons, the abundance and size of staurolite decreases, size and abundance of sillimanite increases, and the abundance of prograde muscovite decreases (is absent near contacts). Kyanite and cordierite were only observed in samples collected within 200 m of a plutonic contact. The lack of such a petrographic break does not necessarily imply synchronicity of regional and contact migmatization, but indicates that retrogression of a regional assemblage did not occur prior to emplacement of the Velfjord plutons. Ion probe studies of the timing of migmatitic events are in progress.

Leucosomes are typically medium-grained, leucocratic, garnet-bearing biotite granodiorite and granite. Garnet, muscovite, and sillimanite are variably present. A few leucosomes contain megacrysts of K-feldspar ± plagioclase that reach 2 to 3 cm in length. Original hypidiomorphic granular texture shows variable degrees of synmagmatic to subsolidus deformation. Quartz is interstitial to sub-poikilitic, with prominent subgrain development. Biotite and muscovite form ragged books. Primary (?) muscovite crystals commonly crosscut the weak foliation and are locally poikilitic. Secondary muscovite replaces K-feldspar and sillimanite. Garnet is poikilitic (or poikiloblastic?) and encloses quartz, or is present as crystal clusters intergrown with quartz. In addition to sillimanite, ilmenite and blocky zircon are accessory minerals.

Contact granites

Most contact granites are K-feldspar-phyric two-mica granite to granodiorite. Some also contain plagioclase phenocrysts. Phenocrysts reach at least 3 cm in length. Groundmass texture is hypidiomorphic granular with variable hypersolidus deformation. The contact granites are typically heterogeneous in terms of the proportion of K-feldspar phenocrysts. Many also contain accessory garnet and sillimanite, some of which occurs in clusters with biotite ± muscovite. The garnet is anhedral and sillimanite ranges from acicular inclusions to sparse equant crystals as much as 0.5 mm across. Ilmenite, zircon, and monazite are accessory minerals; sericite and chlorite are sparse secondary minerals.

Sample N17.91, a garnet-bearing biotite orthopyroxene tonalite, is an unusual contact "granite". Plagioclase phenocrysts up to 2 cm long are set in a groundmass of plagioclase, quartz, and sparse interstitial K-feldspar. Orthopyroxene (opx) crystals are generally ragged and locally have biotite rims. Garnet is anhedral (resorbed?) with straight contacts adjacent to quartz and ragged contacts adjacent to biotite. A symplectic garnet-quartz rim surrounded by biotite separates garnets from adjacent plagioclase phenocrysts. Zircon, ilmenite, and green spinel are accessory minerals.

Analytical methods

Major and trace element contents were determined by x-ray fluorescence analysis at the Norwegian University of Science and Technology (Barnes et al. 1992). Initial wavelength-dispersive electron microprobe analysis of amphibole and plagioclase in the plutonic rocks was done at the Mineralogical Museum, University of Oslo and at Southern Methodist University (Dallas). All other microprobe analyses were done at the Department of Geology and Geophysics, University of Wyoming. Analytical conditions were at a nominal accelerating voltage of 20 kV, beam current of 20 nanoamps (10 for feldspar), with a focused beam. Natural and synthetic standards were used; the data were reduced using the ZAF correction.

Analyses of amphibole, garnet, biotite, and plagioclase used in thermobarometric calculations were, whenever possible, made on adjacent rims. In general, mantle and core compositions were also determined. In migmatitic samples, biotite crystals adjacent to garnet, as well as ones at some distance from garnet, were analyzed.

Mineral compositions

Representative compositions of minerals analyzed for thermobarometric calculations are presented in Tables 2 to 6. Plagioclase anorthite contents are summarized in Table 1 and compositions used in the calculations are given along with the appropriate amphibole or garnet rim composition in Tables 3 and 5. For Al-in-hornblende barometry, plagioclase rim compositions were used. Plagioclase in the migmatitic rocks ranges widely in composition, but zoning in individual samples is commonly weak. Where present, zoning in plagioclase crystals adjacent to garnet is reversed, with slightly more calcic

Table 2. Representative average pyroxene compositions.

Sample	90.27	91.09B	N48.91	N10.91	73.103	91.20	91.24	N10.91	75.01	90.27	N48.91	73.103	N10.91	91.20	91.24	N17.91
	H2	A	A-D	A-D	A-D	S	S	A-D	H1	H2	A-D	A-D	A-D	S	S	tonalite[2]
Pluton[1]	cpx	cpx	cpx	cpx	cpx	cpx	cpx	opx	opx	opx	opx	opx	opx	opx	opx	opx
SiO_2	51.9	52.0	51.6	51.0	51.0	52.4	51.3	53.4	52.5	51.0	50.9	52.9	53.4	52.3	52.9	47.2
TiO_2	0.44	0.17	0.52	0.63	1.02	0.26	0.54	0.20	0.18	0.54	0.32	0.59	0.20	0.13	0.15	0.19
Al_2O_3	1.50	0.92	1.74	3.15	2.99	1.35	3.26	1.56	1.13	0.96	1.00	1.18	1.56	0.87	1.53	3.54
FeO	13.4	12.4	13.8	7.6	11.0	10.9	8.37	17.9	23.1	28.8	29.7	19.8	17.9	25.3	20.5	36.3
MnO	0.64	0.67	0.48	0.23	0.35	0.48	0.25	0.48	0.94	1.09	0.84	0.37	0.48	1.10	0.58	0.59
MgO	12.4	10.8	12.3	14.2	14.0	13.3	13.7	25.4	21.7	17.0	16.9	22.7	25.4	19.8	23.4	11.6
CaO	18.6	22.5	18.6	21.9	19.1	20.9	21.4	0.71	1.10	1.65	1.11	1.82	0.71	0.70	0.98	0.20
Na_2O	0.42	0.73	0.43	0.49	0.52	0.49	0.61	0.02	0.03	0.05	0.02	0.08	0.02	0.03	0.01	0.05
Cr_2O_3	0.04	0.02	0.02	0.08	0.11	0.02	0.06	0.01	n.a.[3]	n.a.	n.a.	0.02	0.01	0.01	0.02	0.04
Total	99.4	100.2	99.6	99.4	100.0	100.1	99.5	99.6	100.6	101.0	100.9	99.5	99.6	100.2	100.0	99.7
Cations per 6 oxygens																
Si	1.974	1.977	1.961	1.909	1.909	1.967	1.919	1.956	1.957	1.953	1.956	1.983	1.956	1.977	1.956	1.895
Ti	0.012	0.005	0.014	0.018	0.028	0.007	0.015	0.005	0.004	0.014	0.009	0.016	0.005	0.004	0.004	0.006
Al	0.067	0.041	0.077	0.139	0.132	0.060	0.144	0.067	0.049	0.042	0.045	0.051	0.067	0.039	0.067	0.168
Fe	0.426	0.395	0.439	0.239	0.343	0.342	0.262	0.547	0.720	0.921	0.955	0.613	0.547	0.801	0.633	1.218
Mn	0.020	0.022	0.014	0.007	0.011	0.015	0.008	0.015	0.029	0.035	0.027	0.011	0.015	0.035	0.018	0.020
Mg	0.703	0.610	0.698	0.794	0.779	0.744	0.762	1.384	1.205	0.969	0.967	1.257	1.384	1.114	1.288	0.696
Ca	0.756	0.919	0.758	0.878	0.766	0.841	0.859	0.028	0.043	0.067	0.045	0.072	0.028	0.028	0.039	0.009
Na	0.030	0.054	0.031	0.036	0.037	0.036	0.044	0.001	0.001	0.003	0.001	0.005	0.001	0.002	0.001	0.004
Cr	0.000	0.001	0.000	0.002	0.002	0.001	0.002	0.000	n.a.	n.a.	n.a.	0.000	0.000	0.000	0.001	0.001
Sum	3.988	4.024	3.992	4.021	4.007	4.013	4.015	4.005	4.008	4.004	4.005	4.008	4.005	4.000	4.007	4.017
Mg#	0.623	0.607	0.614	0.769	0.694	0.685	0.744	0.717	0.626	0.513	0.503	0.672	0.717	0.582	0.670	0.364

[1] Plutons identified as: H1, Hillstadfjellet stage 1; H2, Hillstadfjellet stage 2; A, Aunet; Akset-Drevli, Akset-Drevli; S, Sausfjellet.
[2] Sample N17.91 is a garnet biotite opx tonalite 'contact granite', see text.
[3] n.a. indicates element not analyzed.

Table 3. Representative amphibole analyses.

Sample	75.02	NK74.99	73.138	N40.91	N79.99A	N65.99	91.22A	91.22A	91.37
Pluton[1]	H1	H1	H2	H2	H2	A	S	S	dike
SiO_2	41.7	41.5	40.9	38.9	39.3	42.6	40.5	39.9	40.3
Al_2O_3	11.2	13.1	12.6	13.6	16.0	9.62	13.6	14.8	13.4
FeO	22.4	19.2	21.0	25.5	20.2	20.5	20.7	20.6	22.7
MgO	7.95	8.93	8.22	5.19	7.25	8.76	7.13	6.94	6.85
TiO_2	0.63	0.51	0.41	0.37	0.42	2.04	0.71	0.38	0.75
MnO	0.57	0.28	0.40	1.09	0.40	0.44	0.41	0.48	0.64
CaO	11.4	11.1	11.8	11.2	11.3	11.4	11.9	12.0	11.6
Na_2O	1.52	1.92	1.33	1.48	1.74	1.66	1.04	1.20	1.46
K_2O	1.46	0.77	1.53	1.76	0.67	1.29	1.64	1.67	1.54
Cl	0.08	0.09	0.13	0.14	0.12	0.15	0.12	0.16	0.16
F	0.00	0.00	0.00	0.01	0.00	0.08	0.00	0.00	0.00
Total	98.9	97.4	98.1	99.2	97.4	98.5	97.8	98.1	99.4
Cations per 23 oxygens									
Si	6.404	6.327	6.283	6.095	6.033	6.509	6.246	6.128	6.182
Al	2.023	2.360	2.287	2.502	2.903	1.733	2.467	2.689	2.416
Fe	2.875	2.448	2.692	3.335	2.592	2.616	2.666	2.644	2.910
Mg	1.819	2.030	1.880	1.212	1.660	1.995	1.639	1.592	1.567
Ti	0.072	0.059	0.047	0.044	0.048	0.235	0.082	0.044	0.087
Mn	0.074	0.036	0.053	0.145	0.051	0.057	0.054	0.063	0.084
Ca	1.876	1.817	1.937	1.876	1.856	1.873	1.970	1.982	1.910
Na	0.453	0.568	0.397	0.449	0.517	0.491	0.311	0.356	0.436
K	0.285	0.150	0.299	0.352	0.131	0.252	0.322	0.327	0.302
Cl	0.020	0.023	0.033	0.038	0.030	0.038	0.032	0.041	0.042
F	0.000	0.000	0.000	0.003	0.000	0.039	0.000	0.000	0.000
Total	15.902	15.818	15.907	16.051	15.821	15.838	15.787	15.866	15.934
Mg/(Mg + Fe)	0.388	0.453	0.411	0.267	0.390	0.433	0.381	0.376	0.350
plag. comp.[2]	0.252	0.257	0.281	0.158	0.483	0.232	0.296	0.286	0.378

[1] Plutons are H1, Hillstadfjellet stage 1; H2, Hillstadfjellet stage 2; A, Aunet; S, Sausfjellet.
Sample 91.37 is a granitic dike in the Sausfjellet pluton.
[2] Composition of coexisting plagioclase, given as Ca/(Ca + Na).

Table 4. Representative epidote analyses.

Sample	91.22A	91.37	91.12	N40.91	N40.91	N40.91	N79.99A	NK38.99
Pluton-grain type[1]	S-*p*	dike-*p*	H2-*p*	H2-*p*	H2-si	H2-pi	H2-*p*	H2-s
SiO_2	38.3	38.2	37.4	37.5	38.6	37.5	38.2	38.9
Al_2O_3	25.9	24.4	23.5	24.1	28.3	24.0	25.5	28.6
Fe_2O_3	10.6	13.7	12.7	14.2	7.64	14.3	13.0	8.57
MnO	0.18	0.19	0.35	0.44	0.34	0.43	0.39	0.08
CaO	23.4	23.3	23.1	23.1	23.6	23.5	22.7	24.1
Ce_2O_3	0.11	0.07	0.00	0.14	0.00	0.00	0.03	0.00
Total	98.5	99.9	97.2	99.5	98.4	99.7	99.8	100.3
Cations per 25 oxygens								
Si	5.996	5.958	6.005	5.900	5.973	5.896	5.937	5.930
Al	4.783	4.494	4.443	4.476	5.172	4.439	4.667	5.138
Fe	1.251	1.610	1.533	1.680	0.890	1.692	1.522	0.984
Mn	0.024	0.025	0.047	0.058	0.045	0.058	0.052	0.010
Ca	3.923	3.897	3.979	3.895	3.916	3.954	3.789	3.947
Ce	0.006	0.004	0.000	0.008	0.000	0.000	0.002	0.000
Total	15.984	15.988	16.007	16.018	15.996	16.039	15.968	16.009
Fe/(Fe + Al)	0.207	0.264	0.257	0.273	0.147	0.276	0.246	0.161

[1] Pluton abbreviations as in Table 2. *p* indicates a primary epidote. -s indicates a secondary epidote. -pi indicates a primary epidote inclusion in plagioclase rim, -si indicates a secondary epidote in plagioclase core.

rims than cores. Brief discussions of other analyzed mineral compositions are given below.

Minerals from the plutonic rocks

Pyroxene and olivine. – Average pyroxene compositions are given in Table 2 and plotted in Fig. 3. Clinopyroxene (cpx) is augitic and orthopyroxene (opx) is intermediate in composition (Fig. 3). Cpx and opx from a gabbroic dike in the Akset-Drevli pluton (sample N10.91) are more magnesian than all other samples. Olivine was analyzed from two Akset-Drevli pluton samples; these grains are more Fe-rich (Fo_{57} to Fo_{54}) than would be expected to be in equilibrium with coexisting opx (Fig. 3). Disequilibrium could be due to magma mixing in which olivine and opx were derived from distinct parental magmas. Alternatively, more Mg-rich olivine could have equilibrated with Fe-rich residual liquid during slow cooling, whereas opx did not.

Table 5. Representative garnet rim compositons.

Sample	N17.91	N19.91	91.15A	N14.97B	N14.97B	N14.97A	N92.99A	N92.99A	N112.99	N112.99
SiO_2	37.3	36.5	37.3	37.3	36.9	37.7	37.8	37.1	37.5	37.2
Al_2O_3	20.7	20.1	20.5	20.3	20.4	20.4	21.1	20.9	20.6	20.9
Cr_2O_3	0.02	0.00	0.02	0.00	0.00	0.00	n.a.[3]	n.a.	n.a.	n.a.
FeO	34.4	37.4	32.5	31.4	32.1	34.1	31.6	31.9	36.3	35.5
MnO	1.75	1.66	3.31	5.89	4.83	0.78	3.43	4.14	1.29	2.69
CaO	1.53	0.98	1.50	2.26	1.90	1.47	2.49	1.47	1.59	0.88
MgO	4.51	2.51	4.54	3.06	3.52	4.77	3.86	3.60	2.43	2.48
Total	100.2	99.2	99.7	100.2	99.7	99.2	100.3	99.1	99.7	99.7
Rock type[1]	tonalite	granite	diatex.	diatex.	diatex.	diatex.	diatex.	diatex.	migm.	migm.
Cations per 12 oxygens										
Si	2.987	3.001	3.001	3.009	2.988	3.030	3.013	3.003	3.036	3.017
Al	1.955	1.946	1.943	1.934	1.951	1.932	1.977	1.992	1.968	1.999
Cr	0.001	0.000	0.001	0.000	0.000	0.000	n.a.	n.a.	n.a.	n.a.
Fe	2.304	2.570	2.183	2.117	2.177	2.291	2.106	2.161	2.456	2.407
Mn	0.118	0.116	0.225	0.402	0.331	0.053	0.231	0.284	0.089	0.185
Ca	0.131	0.086	0.129	0.195	0.165	0.127	0.213	0.128	0.138	0.077
Mg	0.539	0.307	0.545	0.367	0.425	0.572	0.458	0.434	0.294	0.300
Total	8.035	8.026	8.027	8.024	8.037	8.004	7.998	8.001	7.980	7.984
X (gross)	0.042	0.028	0.042	0.063	0.053	0.042	0.071	0.042	0.046	0.026
X (pyrope)	0.174	0.100	0.177	0.119	0.137	0.188	0.152	0.144	0.099	0.101
X (alm)	0.745	0.835	0.708	0.687	0.703	0.753	0.700	0.719	0.825	0.811
X (spess)	0.038	0.038	0.073	0.130	0.107	0.017	0.077	0.094	0.030	0.062
Fe/(Fe + Mg)	0.810	0.893	0.800	0.852	0.837	0.800	0.821	0.833	0.893	0.889
An (plag)[2]	0.33	0.30	0.66	0.43	0.46	0.40	0.39	0.38	0.26	0.26

[1] Samples N17.91 and N19.91 are contact 'granites'. Other samples are diatexite (diatex.) and layer-bound migmatite (migm.).
[2] Composition of coexisting plagioclase, given as Ca/(Ca + Na).
[3] n.a. indicates not analyzed.

Table 6. Representative biotite analyses.

Sample	N17.91	N19.91	N103.99	91.15A	N14.97A	N14.97B	N92.99A	N112.99A	N51.91B
SiO_2	35.5	34.9	36.3	35.9	36.2	35.5	36.5	34.8	35.2
Al_2O_3	15.9	19.7	20.8	20.1	19.8	19.9	19.8	20.4	19.9
TiO_2	4.35	3.30	1.26	2.55	2.28	2.90	1.63	1.72	1.80
FeO	22.1	20.5	15.9	17.7	16.0	17.7	16.3	21.8	21.9
MgO	10.1	8.20	13.2	11.1	12.2	10.3	12.6	9.36	8.57
MnO	0.04	0.02	0.07	0.09	0.03	0.15	0.09	0.00	0.03
CaO	0.01	0.00	0.01	0.00	0.02	0.00	0.00	0.00	0.00
Na_2O	0.03	0.10	0.35	0.17	0.30	0.22	0.16	0.18	0.22
K_2O	9.92	10.07	9.15	9.67	9.31	9.82	9.12	9.22	9.50
F	0.15	0.29	0.00	0.01	0.00	0.00	0.34	0.00	0.12
Cl	0.14	0.04	0.05	0.05	0.01	0.02	0.09	0.05	0.27
Total	98.2	97.0	97.0	97.2	96.2	96.4	96.4	97.5	97.4
Rock type	tonalite	granite	diatex. dike	diatex.	diatex.	diatex.	diatex.	migm.	migm.
Cations per 22 oxygens									
Si	5.363	5.280	5.305	5.304	5.351	5.304	5.397	5.230	5.317
Al	2.836	3.514	3.589	3.496	3.457	3.502	3.440	3.608	3.541
Ti	0.493	0.375	0.138	0.284	0.253	0.326	0.182	0.194	0.204
Fe	2.795	2.585	1.939	2.185	1.985	2.209	2.008	2.737	2.766
Mg	2.274	1.847	2.879	2.447	2.693	2.293	2.781	2.094	1.929
Mn	0.005	0.003	0.008	0.011	0.004	0.018	0.011	0.000	0.004
Ca	0.001	0.000	0.002	0.000	0.003	0.000	0.000	0.000	0.000
Na	0.009	0.030	0.099	0.050	0.086	0.064	0.047	0.053	0.064
K	1.910	1.941	1.706	1.824	1.756	1.872	1.718	1.766	1.832
F	0.069	0.138	0.000	0.003	0.000	0.000	0.160	0.000	0.057
Cl	0.036	0.010	0.012	0.013	0.002	0.004	0.023	0.013	0.068
Total	15.790	15.722	15.677	15.617	15.591	15.591	15.767	15.695	15.782
Fe/(Fe + Mg)	0.551	0.583	0.402	0.472	0.424	0.491	0.419	0.567	0.589

Amphibole. – In the classification of (Leake et al. 1997), amphiboles are predominantly ferropargasite and ferro-edenite (Fig. 4). Amphiboles from relatively Mg-rich samples also encompass edenitic and pargasitic compositions. Amphibole from the Hillstadfjellet, Akset-Drevli, and Aunet plutons are Na-rich relative to amphibole from the Sausfjellet pluton, with >0.4 cations per formula unit (pfu) in the former plutons and <0.44 cations pfu in the latter (Table 3). Among samples that show core-to-rim zoning, Al is generally enriched in the rims relative to the cores.

Epidote. – Epidote compositions (Table 4) show little variation within single crystals except adjacent to allanite

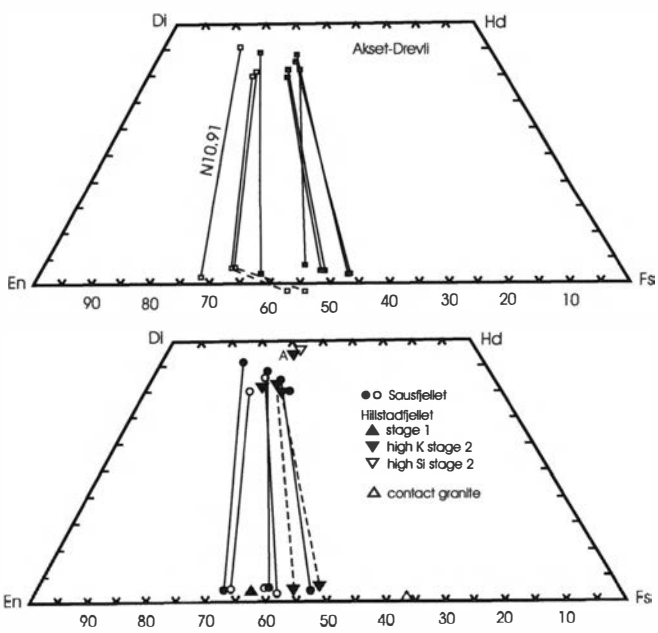

Fig. 3. Pyroxene compositions plotted in the pyroxene quadrilateral. Compositions of coexisting olivine are shown along the base of the upper figure.

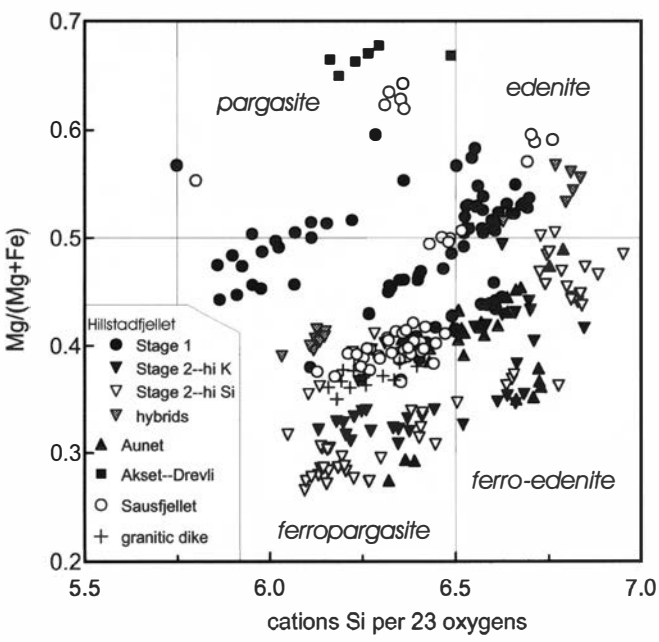

Fig. 4. Classification of amphiboles from the Velfjord plutons and related granitic dikes (Leake et al. 1997).

cores. Petrographically, epidote is present as primary and secondary crystals. The pistacite component [$Ps = Fe^{+3}/(Fe^{+3} + Al)$] of primary epidote varies from 0.23 to 0.29 (ave. 0.26), whereas the Ps component of secondary crystals ranges from 0.15 to 0.26 (ave. 0.21). In a sample from the Hillstadfjellet pluton (N40.91) clear epidote inclusions in the core of a plagioclase phenocrysts have a Ps content of 0.19, whereas pale yellow-green epidote from the plagioclase rim has a Ps value of 0.28. Primary epidote typically has Ps contents in the 0.23 to 0.29 range (Zen & Hammarstrom 1984), whereas epidote that replaces plagioclase has Ps values from 0.0 to 0.24 (see Brandon et al. 1996).

Minerals from migmatites and contact granites

Garnet. – Garnets from migmatitic wall rocks and contact granites are predominantly almandine (Table 5). The almandine component ranges from 69% to 84% (molecular), grossular component from 1% to 9%, pyrope component from 7% to 21%, and spessartine component from 1% to 15%. Garnets from the *contact granites and diatexites* show little zoning. For example, the value of Fe/(Fe + Mg) in garnet, which varies from 0.68 to 0.92 among all analyzed samples, typically has a standard deviation of less than 0.02 in an individual sample. Such zoning as is apparent involves a 2–3% increase in grossular component in garnet rims (Table 5). In such crystals these rims must be discontinuous because other analyses of rims from the same crystals are identical to the cores.

In contrast, garnets from a *stromatic migmatite* collected 1.5 km from the Sausfjellet pluton (sample N51.91B) show the opposite sense of zoning, with a decrease in grossular component from core to rim.

Biotite. – Representative biotite analyses are given in Table 6. Individual biotite crystals lack compositional zoning. However, biotites adjacent to garnet typically have lower values of Fe/(Fe + Mg) than those at some distance from garnet grains. The differences in Fe/(Fe + Mg) range from 0.04 to 0.10. The biotites are relatively Al-rich (Al >3.4 pfu), as is expected of biotite from peraluminous compositions. An exception to this is biotite from the opx-bearing contact granite (N17.91) in which Al contents are <3.0 pfu.

Temperature and pressure estimates from plutonic rocks

Pyroxene – olivine equilibria

Temperature estimates were made on the basis of two-pyroxene and olivine + pyroxene equilibria using the QUILF4 program (Frost & Lindsley 1992; Lindsley & Frost 1992). Ferric iron contents were estimated by recalculation to four cations (Cebriá Gómez 1990). Temperature calculated on the basis of two-pyroxene – olivine equilibria for samples from the Akset-Drevli pluton were 1060°C. Estimates made on the basis of two-pyroxene equilibria range from 900°C to 1015°C for Sausfjellet, 790° to 1070° for Akset-Drevli, and 810°C to 970°C for Hillstadfjellet.

Apatite saturation thermometry

The apatite saturation thermometer (Harrison & Watson 1984; Watson & Harrison 1984) permits calculation of the temperature at which apatite would be stable in a melt of the composition of a particular rock. This method assumes that apatite stability was not controlled by kinetic factors (Bacon 1989) and was not a cumulate phase. It also assumes that a given rock composition is representative of a melt composition.

The thermometric data suggest apatite saturation in the Hillstadfjellet pluton at about 975°C, in the Akset-Drevli pluton at about 1020°C, and in the Sausfjellet pluton at about 950°C. Although these temperatures are consistent with those determined with pyroxene-olivine equilibria, they do not necessarily indicate the temperature of emplacement.

Amphibole – plagioclase equilibria

The Al content of amphibole in equilibrium with plagioclase, quartz, biotite, Fe-Ti oxide, titanite, and K-feldspar has been shown to be a function of the pressure of crystallization (Hammarstrom & Zen 1986; Hollister et al. 1987; Schmidt 1992). Furthermore, Holland & Blundy (1994) showed that the compositions of coexisting amphibole and plagioclase are controlled by temperature-dependent equilibria. Anderson & Smith (1995) combined the two schemes to develop a temperature-corrected Al-in-hornblende barometer.

Several samples from the Velfjord plutons contain the appropriate equilibrium assemblage and others lack only K-feldspar; however, Anderson & Smith (1995) indicated that the presence or absence of K-feldspar and titanite had no apparent effect on the results of the barometer. Application of the Anderson & Smith (1995) barometer results in P estimates that range from 4.1 to 7.7 kbar (Table 7). Amphiboles that yield pressure estimates ≥5.7 kbar are characteristically blue-green. Among the three samples that yield pressures <5.7 kbar, the amphiboles are olive green with blue-green rims a few microns wide. For two of these samples (91.13 and 91.14), it was not possible to determine rim compositions. Textural study of the other sample (gabbro NK74.99) suggests that amphibole was not in equilibrium with the complete buffer assemblage at the solidus.

Temperature estimates based on the pressure-corrected Holland & Blundy (1994) algorithm (Anderson & Smith 1995) range from 673°C to 757°C (Table 7). These values are consistent with final amphibole-plagioclase equilibrium at near-solidus conditions.

Table 7. Results of Al-in-hornblende barometry.

Sample	Setting	P (kbar)[1]	sd	P (kbar)[2]	sd	T (C)[3]	sd	N[4]	Notes[5]
Sausfjellet									
91.37	Granitic dike	7.6	0.4	7.0	0.3	710	20	8	Primary Ep
91.22A	Quartz diorite	7.9	0.7	7.7	0.7	686	15	16	
73.65	Quartz diorite	7.4	0.5	6.6	0.5	725	10	4	Primary Ep
Hillstadfjellet, Stage 1									
75.02	Stage 1, Hill.	6.2	0.6	5.9	0.6	696	13	11	Ilm primary; Ttn secondary
NK74.99	Stage 1, Hill.	7.5	1.0	6.8	0.9	720	13	11	Lacks Kfs
Hillstadfjellet, Stage 2									
73.138	Monzodiorite	8.3	0.6	7.2	0.5	734	20	8	Ilm & Ep primary; Ttn secondary
91.12	Quartz monzonite	7.3	0.4	6.9	0.3	701	21	10	
91.13	Quartz monzonite	4.5	0.2	4.5	1.5	673	8	4	Secondary Ttn
91.14	Quartz monzonite	4.3	0.2	4.1	0.5	700	18	5	Lacks Ttn
NK17.99	Monzonite	5.0	0.4	4.1	0.7	736	19	9	Hbl after Cxp & Opx
Hillstadfjellet, Stage 2 rocks in contact zones									
N40.91	Quartz monzonite	7.7	1.0	7.4	0.9	693	16	18	Primary Ep
N66.99	Hill. contact hybrid	6.6	1.6	5.7	1.4	731	6	5	Primary Ep
N79.99A	Hill. contact hybrid	8.7	2.4	7.0	2.0	757	14	11	Primary Ep; lacks Ttn, Kfs
Aunet pluton and dikes of Aunet-type monzonite									
90.06	Monzonite	6.9	0.2	6.8	0.2	678	3	2	
91.09B	Monzonite	4.6	0.2	4.1	0.3	712	10	4	Hbl after Cxp & Opx
N65.99	Monzonite dike	5.5	0.6	4.8	0.6	726	19	8	Hbl after Cxp & Opx
Samples lacking equilibrium assemblage or clearly hybrid									
75.01	Hillstadfjellet gabbro	5.8	0.5	1.9	0.7	849	24	6	Lacks Qtz, Ttn, Kfs
90.27	Hillstadfjellet monzodiorite	4.2	0.1	3.9	0.3	700	15	3	Lacks Qtz
NK38.99	Hillstadfjellet gabbro	11.3	0.8	10.0	0.9	730	27	12	Lacks Qtz, Ttn, Kfs
91.24	Sausfjellet diorite	7.3	0.3	4.3	0.5	812	10	3	Lacks Qtz, Bt, Ttn, Kfs
Mingled rocks in Hillstadfjellet contact zone									
91.10A	Quartz diorite	9.3	0.9	9.4	0.8	661	21	5	Lacks Ttn, Kfs
91.10B	Quartz diorite	9.3	0.1	9.5	0.2	656	19	3	Lacks Ttn, Kfs

[1] Pressure estimates based on rim compositions and Schmidt (1992) calibration; all Fe as Fe^{2+}.
[2] Pressure estimates based on rim compositions and Anderson & Smith (1995) calibration.
[3] Temperature setimate based on Holland & Blundy (1994).
[4] Number of samples used in calculation.
[5] Mineral abbreviations are Kfs, K-feldspar; Hbl, calcic amphibole; Cpx, augite; Opx, orthopyroxene; Bi, biotite; Ttn, titanite; Qtz, quartz; Ep, epidote.

Epidote stability

Experimental studies of epidote stability (Naney 1983; Schmidt 1992, 1993) show that magmatic epidote in equilibrium with amphibole is stable at pressures greater than about 6 kbar. The widespread presence of such primary epidote in quartz-bearing rocks of the Hillstadfjellet and Sausfjellet plutons is consistent with the Al-in-hornblende pressure estimates >5.7 kbar cited above.

Temperature and pressure estimates from migmatitic rocks and contact granites

Zircon saturation temperatures

Zircon saturation thermometry (Watson 1979; Watson & Harrison 1983) can be applied to the leucosomes in the wall rock migmatites and the contact granites. This method assumes that the bulk rock compositions represent melt compositions and that no zircon in the rock is residual. Neither assumption is fully justified. For example, residual zircon can be entrained in both leucosomes and contact granites. In addition, if melting and melt extraction is rapid, zircon may not reach equilibrium with the partial melt (Watson 1996). Finally, leucosomes may be partial cumulates. Entrainment of residual zircon results in higher T estimates than expected, whereas lack of equilibrium and accumulation of other crystals result in lower T estimates. Given these caveats, the contact granites yield zircon saturation temperatures from 780°C to 900°C and granitic leucosomes yield temperatures from 710°C to 780°C.

GASP barometry

Migmatitic metapelites adjacent to the Velfjord plutons and some contact granites contain the assemblage garnet + sillimanite ± kyanite + biotite + plagioclase + quartz. This 'GASP' assemblage can be described by two equilibria: the Mg-Fe exchange between biotite and garnet and the discontinuous reaction:

$$3CaAl_2Si_2O_8 \longleftrightarrow Ca_3Al_2Si_3O_{12} + 2Al_2SiO_5 + SiO_2$$

anorthite grossular Als quartz.

Simultaneous solution of these reactions results in an estimate of the P and T of equilibrium. The reactions were solved using the program TWQ (Berman 1991) and the

database and end member properties of Berman (1988, 1990). Solution models used were those of Berman & Koziol (1991) for garnet, McMullin et al. (1991) for biotite, and Fuhrman & Lindsley (1988) for plagioclase.

The results of GASP thermobarometry on contact granites and migmatites vary widely (Fig. 5). Because garnets in many migmatitic samples have rims with variable composition, it is possible to determine more than one pressure for a single sample. The highest pressure estimates (~7 to 9 kbar) result from the use of the most Ca-rich garnet rim compositions and plot on or near the kyanite = sillimanite boundary (Fig. 5), which is consistent with the presence of early kyanite in some samples. It is noteworthy that the sample that yields $P \geq 9$ kbar (sample N103.99) is a diatexitic dike in the Sausfjellet pluton. Thus, this sample may have equilibrated at higher P and risen to its depth of emplacement.

In cases where plagioclase adjacent to garnet is zoned, reverse zoning is most common. The lower An core compositions result in this highest pressure estimates, which is consistent with the proposed P-T path (see below).

Many samples give GASP results in the 4 to 5 kbar range and a few give results that plot in the andalusite stability field (Fig. 5). Because the GASP thermobarometer is commonly affected by re-equilibration of biotite during retrogression, and because andalusite is absent in these samples, the GASP results are thought to reflect low-T equilibration of biotite. This is supported by the fact that the garnet – plagioclase equilibrium boundary for these samples projects toward high-*P* values at higher temperatures, it is the garnet – biotite equilibrium that has been reset. For all other samples, the equilibration temperature determined by GASP calculations ranges from 620°C to 730°C.

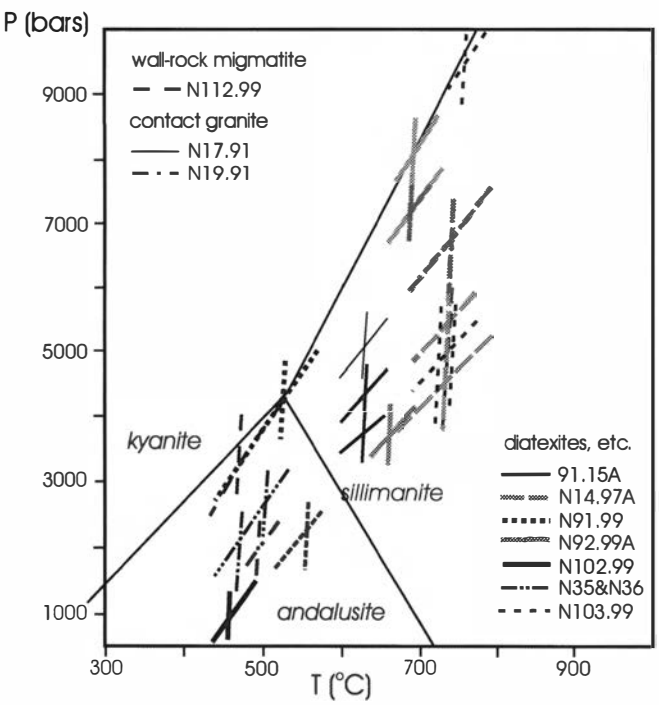

Fig. 5. Results of GASP thermobarometry. Line intersections represent solution of the garnet-plagioclase-aluminosilicate-quartz equilibrium with Fe-Mg exchange equilibrium among garnet and biotite.

Discussion

A proposed P-T-t path

On the basis of Al-in-hornblende barometry and the presence of magmatic epidote, the pressure of emplacement of the Velfjord plutons is thought to be ≥7 kbar (Fig. 6A). If this is the case, the migmatitic wall rocks should also record pressures near 7 kbar.

The migmatitic wall rocks adjacent to the plutons contain a metamorphic assemblage that is unlikely to represent a single equilibrium P and T. This is particularly apparent in samples that contain kyanite, sillimanite, garnet, and cordierite. In the melting interval, mutual stability of kyanite and cordierite is unlikely (e.g. Spear et al. 1999; Fig. 6A). The assemblage suggests either a polymetamorphic history or metamorphism along a P-T loop. The latter interpretation is preferred because the two discrepant minerals, kyanite and cordierite, are absent in pelitic rocks collected outside the contact aureole of the plutons. This in turn suggests that these minerals grew in response to contact metamorphism (and anatexis) associated with Velfjord plutonism. Thus the metamorphic history recorded in the contact migmatites is thought to reflect variations in P and T during the late Ordovician intrusive event.

A recent contribution by Spear et al. (1999) outlined the equilibria that are likely to control melting of pelitic rocks in which a free H_2O phase is absent during anatexis (dehydration melting). Their petrogenetic grid (Fig. 6A) provides a useful context for discussion of the various estimates of P and T. Features of the contact migmatites that must be explained include:

1. Localized occurrence of kyanite and cordierite adjacent to the plutons and the fact that these minerals probably were out of equilibrium with each other.
2. Local growth of K-feldspar megacrysts in early stages of migmatization.
3. Growth of sillimanite in multiple episodes.
4. Discontinuous zoning of garnet rims and preservation of rim sections, some of which apparently grew at $P \geq 7$ kbar and others that grew at ~4 to 5 kbar.
5. Evidence for resorption of garnet.
6. Evidence for interstitial intergrowth of biotite + sillimanite.
7. Local retrogression of sillimanite and feldspar to muscovite, especially in leucosomes and migmatites collected at some distance from the pluton.
8. Late-stage growth of fine-grained prisms of staurolite.

A clockwise P-T metamorphic path can explain these observations. Specific evidence that points to a clockwise,

rather than anti-clockwise, P-T path can be summarized as follows. Kyanite formed early in the metamorphic history, as shown by development of sillimanite beards on ragged kyanite and by kyanite inclusions in cordierite. Cordierite was a late-stage mineral, as shown by its idiomorphic to intergranular habit and its concentration in leucosomes. In samples in which residual plagioclase is zoned, the most sodic zones are in the cores or mantles of the crystals, not the rims. Reverse zoning is consistent with a clockwise path, whereas normal zoning suggests an anti-clockwise path.

Possible clockwise P-T paths are illustrated in Fig. 6B and are described below. So little is known about the regional pre-intrusion metamorphic gradient that the P-T conditions of the wall rocks prior to magmatism cannot yet be properly determined. Further work in this regard is in progress. However, because P of emplacement can be independently estimated by Al-in-hornblende barometry, it is possible to determine the initial P-T conditions of contact melting with reasonable accuracy.

As the Velfjord magmas were emplaced, the wall rocks immediately adjacent to the plutons were heated to temperatures >700°C. Kyanite grew in the hottest rocks, probably by the reaction (Spear, 1993):

staurolite + chlorite = biotite + kyanite + H2O

at temperatures above about 625 °C.

If interstitial vapor was present, melting was initiated along reaction I (see Fig. 6B); otherwise melting occurred by reactions II and III. Each of the latter two reactions produces K-feldspar. Formation of K-feldspar-phyric leucosomes can be explained by partial melting according to these reactions, and the K-feldspar-phyric contact granites probably originated in the same way. At the highest temperatures of contact melting, reaction IV produced opx and sillimanite. It seems likely that the biotite opx tonalite 'contact granite' sample N17.91 resulted from melting by this reaction. The higher temperature implied by the assemblage in sample N17.91 suggests that the magma formed in a deeper, hotter part of the contact zone and rose to the level of emplacement.

Following initial melting at high-P, conditions must have changed such that cordierite became stable. Most probably, this involved decompression (due to exhumation?). As reaction V was crossed, biotite and sillimanite reacted to form garnet, cordierite and melt (Fig. 6B). In the highest grade diatexites, garnet has a value of Fe/(Fe + Mg) = 0.7. This composition of garnet in equilibrium with cordierite, biotite, sillimanite, K-feldspar, and melt suggests conditions of cordierite growth of slightly greater than 750°C at about 5.5 kbar (Fig. 6B). Samples collected at greater distances from the plutons would have followed a tighter P-T loop and would not have entered the cordierite stability field.

The retrograde path requires precipitation of biotite and sillimanite, but not cordierite. Crystallization (isobaric cooling?) on equilibria III and V would result in resorption of garnet, cordierite, and K-feldspar and precipitation of biotite and sillimanite as interstitial, intergrown patches. Crystallization at about 4 to 5 kbar is consistent with the numerous P-T estimates from these rocks on the basis of GASP thermobarometry (Fig. 5). The widespread appearance of euhedral, interstitial staurolite in these migmatites suggests that staurolite was stable at the solidus. Spear et al. (1999) proposed a staurolite dehydration reaction:

staurolite + muscovite = garnet + biotite + Al_2SiO_5 + liquid,

and proposed a range of pressure for this reaction from about 5 to 7 kbar. The validity of this reaction awaits further experimental and field study.

Samples from which significant amounts of melt had been extracted underwent retrogression without evolution of significant H_2O (e.g. Spear et al. 1999). Such rocks would be effectively isolated from further down-temperature retrogression because of the lack of H_2O. In contrast, samples that contained a significant volume of anatectic melt probably evolved significant H_2O during crystallization, which was then available for reaction with sillimanite and K-feldspar to form muscovite. This is indeed the case adjacent to the Velfjord plutons. Sillimanite- and garnet-rich (restitic) samples typically contain little or no retrograde muscovite. However, leucosomes and leucosome-rich diatexites commonly display significant retrogression in which muscovite replaces feldspars, sillimanite, and cordierite. This abundant late-stage muscovite probably results from evolution of H_2O from the leucosome melt at the solidus.

Thermal energy for wall rock anatexis

Migmatization due to heat from the Velfjord plutons affects rocks at least 1000 m from the pluton contacts. This implies emplacement of the plutonic magmas at high T, or initial high wall rock temperature, or both. Available data for olivine-pyroxene equilibria suggest pluton emplacement temperatures $\leq$1070°C. Such temperatures are too low to represent crystal-free liquidi of H_2O-poor magmas, which are in the range of 1250°C for the Akset-Drevli pluton (K. Chapman and C. Barnes, research in progress). Thus, the temperature estimates may reflect cation exchange among pyroxene $\pm$ olivine during cooling. Alternatively, the plutons could have been emplaced as crystal-rich mushes. However, the presence of fine-grained mafic dikes in the wall rocks suggests near-liquidus emplacement of at least some of the magmas, thereby supporting higher emplacement temperatures.

A complete understanding of the heat transfer to the wall rocks and its effects on migmatization depends on more detailed two-pyroxene thermometry. These data will permit modeling of the thermal evolution of the magmas and their wall rocks.

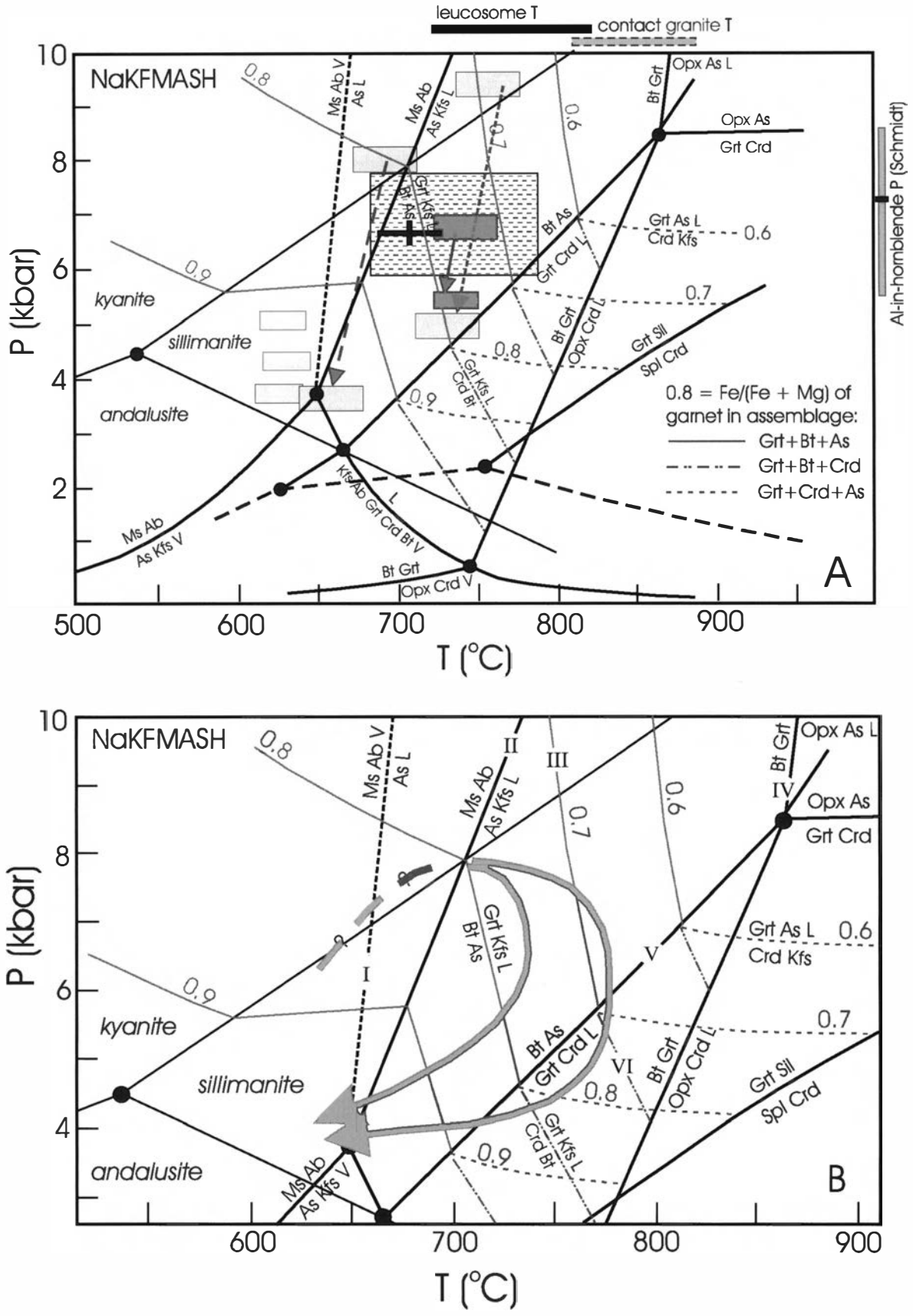

Fig. 6. Results of P-T estimates compared to a petrogenetic grid for dehydration partial melting of metapelites (after Spear et al. 1999). (A) Shaded rectangles indicate the location of P-T estimates from GASP thermobarometry that are consistent with the mineral assemblage. The large rectangle with patterned fill is the range of P and T estimates for emplacement of the Velfjord plutons using the temperature-corrected Al-in-hornblende barometer (Anderson & Smith 1995) and the hornblende-plagioclase thermometer of Holland & Blundy (1994). The black bar in this box represents the average of the results. The bar on the right side of the diagram gives the range of pressures determined using the Schmidt (1992) calibration of the Al-in-hornblende barometer, the black bar is the average. Bars at the

Implications for regional geology

This work shows that a number of thermobarometric methods can be used to determine the conditions of emplacement of the Bindal Batholith. In addition, it shows that at least some of the older plutons in the Batholith underwent nearly isothermal decompression from about 7 kbar to 4 to 5 kbar. The duration of such a decompression event is uncertain, but was probably rapid in view of the fact that the migmatitic wall rocks remained above their solidi.

Radiometric ages of Bindal plutons range from ~450 Ma to ~430 Ma (Nordgulen et al. 1993) with some plutons as old as 481 Ma (Pedersen et al. 1999). If exhumation following ~448 Ma emplacement of the Velfjord plutons were rapid, then younger plutons in the Batholith would have been emplaced at lower pressure. The success of Al-in-hornblende barometry in this work suggests that judicious application of the barometer on other samples of the Bindal Batholith can provide important constraints on the P-T history of the entire HNC during late Ordovician and early Silurian time.

At present it is not certain what tectonic event was responsible for burial of the HNC prior to emplacement of the Velfjord magmas. The host rocks to the plutons are in thrust contact with low-to medium-grade rocks to the east (Fig. 2) such that juxtaposition of these units could be responsible for the high emplacement pressure. However, previous workers indicated that a break in metamorphic conditions exists between the structurally higher rocks and the host rocks to the Velfjord plutons. Further work must be focused on the nature of this contact and the age of movement along it. At least two possible explanations are possible. First, a metamorphic break may not exist between the two thrust sheets. It is possible that the apparent higher grade of the host rocks of the Velfjord plutons is a 'regional contact metamorphic' effect. Second, if a metamorphic break does exist, the last displacement on the thrust could have been in a low-angle normal sense, possibly reactivation of an original thrust fault. This would explain the normal sense of displacement (low-grade over high-grade) and could provide a mechanism for exhumation of the underlying high-T unit.

Summary

The Velfjord plutons were emplaced into carbonate and pelitic host rocks at about 448 Ma. The pressure of emplacement was approximately 7 kbar. Heat transferred from the plutons to the host rocks resulted in dehydration partial melting of the pelites, which produced melts capable of crystallizing K-feldspar megacrysts. Some of these anatectic magmas escaped the zone of melting, thereby depleting the source rocks in fertile components and H_2O. A few of the anatectic magmas accumulated and solidified along the contacts of the plutons to form 'contact granites'.

Nearly isothermal decompression followed, such that high-T wall rock migmatites entered the stability field of cordierite. In contrast, lower-T wall rocks at greater distances from the plutons did not reach cordierite stability. Cooling and solidification occurred at 4 to 5 kbar and resulted in interstitial intergrowths of biotite and acicular sillimanite.

The results of this study imply rapid exhumation of the HNC following emplacement of the Velfjord plutons. Thermobarometric studies on younger plutons in the Bindal Batholith should provide a means to test and better quantify this P-T-t path.

Acknowledgements. – We are grateful to Øystein Nordgulen for his interest and input during all stages of this project, to Melanie Barnes for her assistance in the field, and to Susan Swapp and Håkon Austrheim for their assistance with microprobe analysis. Frank Spear, Reidar Trønnes, and Rune B. Larsen provided very helpful reviews. This research was initially funded by a grant from the Nansenfundet to Prestvik and by National Science Foundation grant EAR-9814280.

Manuscript received May 2000

References

Anderson, J. L. & Smith, D. R. 1995: The effects of temperature and fO_2 on the Al-in-hornblende barometer. *American Mineralogist 80,* 549–559.

Bacon, C. R. 1989: Crystallization of accessory phases in magmas by local saturation adjacent to phenocrysts. *Geochimica et Cosmochimica Acta 53,* 1055–1066.

Barnes, C. G., Prestvik, T., Nordgulen, Ø. & Barnes, M. A. 1992: Geology of three dioritic plutons in Velfjord, Nordland. *Norges geologiske undersøkelse Bulletin 423,* 41–54.

Berman, R. G. 1988: Internally-consistent thermodynamic data for stoichiometric minerals in the system Na_2O-K_2O-CaO-MgO-FeO-Fe_2O_3-Al_2O_3-SiO_2-TiO_2-H_2O-CO_2. *Journal of Petrology 29,* 445–522.

Berman, R. G. 1990: Mixing properties of Ca-Mg-Fe-Mn garnets. *American Mineralogist 75,* 328–344.

Berman, R. G. 1991: Thermobarometry using multiequilibrium calculations: a new technique with petrologic applications. *Canadian Mineralogist 29,* 833–855.

Berman, R. G. & Koziol, A. M. 1991: Ternary excess properties of grossular-pyrope-almandine garnets and their influence in geothermobarometry. *American Mineralogist 76,* 1223–1231.

Birkeland, A., Nordgulen, Ø., Cumming, G. L. & Bjørlykke, A. 1993: Pb-Nd-Sr isotopic constraints on the origin of the Caledonian Bindal Batholith, central Norway. *Lithos 29,* 257–271.

Brandon, A., Creaser, R. & Chacko, T. 1996: Constraints on rates of granitic magma transport from epidote dissolution kinetics. *Science 271,* 1845–1848.

top of the diagram indicate the range of zircon saturation T estimates for migmatitic leucosomes and contact granites. Isopleths in the diagram are labeled according to the composition of garnet in equilibrium with the appropriate assemblage. (B) P-T paths for contact migmatites. Question marks indicate uncertainty in the path prior to beginning of partial melting. The higher temperature loop corresponds to migmatitic rocks nearest to the plutons. Melting initially involved reaction III, but during decompression, reactions V and VI(?) produced cordierite. The lower temperature loop corresponds to migmatitic rocks >100 m from the plutons. Because these rocks did not reach such high temperatures, their decompression paths failed to intersect the cordierite stability field. Phase abbreviations are: Ms, muscovite; ab, albite; As, aluminosilicate; Kfs, K-feldspar; Bt, biotite; Grt, garnet; Opx, orthopyroxene; Crd, cordierite; Spl, spinel; Sil, sillimanite; L, silicate melt; V, aqueous fluid.

Cebriá Gómez, J. M. 1990: PX: A program for pyroxene classification and calculation of end-members. *American Mineralogist 75,* 1426–1427.

Frost, B. R. & Lindsley, D. H. 1992: Equilibria among Fe-Ti oxides, pyroxenes, olivine, and quartz: Part II. Application. *American Mineralogist 77,* 1004–1020.

Fuhrman, M. L. & Lindsley, D. H. 1988: Ternary-feldspar modeling and thermometry. *American Mineralogist 73,* 201–216.

Gautneb, H. & Roberts, D. 1989: Geology and petrochemistry of the Smøla-Hitra Batholith, Central Norway. *Norges geologiske undersøkelse Bulletin 416,* 1–24.

Gustavson, M. 1978: Caledonides of north-central Norway. *Geological Survey of Canada, Paper 78- 13,* 25–30.

Hammarstrom, J. M. & Zen, E. 1986: Aluminum in hornblende: an empirical igneous geobarometer. *American Mineralogist 71,* 1297–1313.

Harrison, T. M. & Watson, E. B. 1984: The behavior of apatite during crustal anatexis: Equilibrium and kinetic considerations. *Geochimica et Cosmochimica Acta 48,* 1467–1477.

Holland, T. & Blundy, J. 1994: Non-ideal interactions in calcic amphiboles and their bearing on amphibole-plagioclase thermometry. *Contributions to Mineralogy and Petrology 116,* 433–447.

Hollister, L. S., Grissom, G. C., Peters, E. K., Stowell, H. H. & Sisson, V. B. 1987: Confirmation of the empirical correlation of Al in hornblende with pressure of solidification of calc-alkaline plutons. *American Mineralogist 72,* 231–239.

Kollung, S. 1967: Geologiske undersøkelser i det sørlige Helgeland og nordlige Namdal. *Norges geologiske undersøkelse Bulletin 254,* 95 pp.

Leake, B., et al. 1997: Nomenclature of amphiboles: rReport of the Subcommittee on Amphiboles of the International Mineralogical Association, Commission on New Minerals and Mineral Names. *American Mineralogist 82,* 1019–1037.

Lindsley, D. H. & Frost, B. R. 1992: Equilibria among Fe-Ti oxides, pyroxenes, olivine, and quartz: Part I. Theory. *American Mineralogist 77,* 987–1003.

McMullin, D., Berman, R. G. & Greenwood, H. J. 1991: Calibration of the SGAM thermobarometer for pelitic rocks using data from phase equilibrium experiments and natural assemblages. *Canadian Mineralogist 29,* 889–908.

Myrland, R. 1972: Velfjord. Beskrivelse til det berggrunns-geologiske gradteigskart I 18-1:100,000. *Norges geologiske undersøkelse 274,* 30 pp.

Naney, M. T. 1983: Phase equilibria of rock-forming ferromagnesian silicates in granitic systems. *American Journal of Science 283,* 993–1033.

Nordgulen, Ø. 1993: A summary of the petrography and geochemistry of the Bindal Batholith. *Geological Survey of Norway, Report 92.111.*

Nordgulen, Ø., Fjeldheim, T., Ihlen, P. M., Nissen, A. L. & Solli, A. 1992 *Vevelstad berggrunnskart 1826-3, 1:50,000, Norges geologiske undersøkelse.*

Nordgulen, Ø., Bickford, M., Nissen, A. & Wortman, G. 1993: U-Pb zircon ages from the Bindal Batholith, and the tectonic history of the Helgeland Nappe Complex, Scandinavian Caledonides. *Journal of the Geological Society, London 150,* 771–783.

Nordgulen, Ø. & Schouenborg, B. 1990: The Caledonian Heilhornet pluton, north-central Norway: geological setting, radiometric age and implications for the Scandinavian Caledonides. *Journal of the Geological Society, London 147,* 439–450.

Nordgulen, Ø. & Sundvoll, B. 1992: Strontium isotope composition of the Bindal Batholith, Central Norwegian Caledonides. *Norges geologiske undersøkelse Bulletin 423,* 19–39.

Pedersen, R.-B., Nordgulen, Ø., Barnes, C. G., Prestvik, T. & Barnes, M. 1999: U-Pb dates from dioritic and granitic rocks in Velfjord, north-central Norway. *Geonytt 26,* 81.

Schmidt, M. W. 1992: Amphibole composition in tonalite as a function of pressure: an experimental calibration of the Al-in-hornblende barometer. *Contributions to Mineralogy and Petrology 110,* 304–310.

Schmidt, M. W. 1993: Phase relations and compositions in tonalite as a function of pressure: an experimental study at 650°C. *American Journal of Science 293,* 1011–1060.

Schmidt, M. W. & Thompson, A. B. 1996: Epidote in calc-alkaline magmas: an experimental study of stability, phase relationships, and the role of epidote in magmatic evolution. *American Mineralogist 81,* 462–474.

Spear, F. 1993: Metamorphic phase equilibria and pressure-temperature-time paths. *Mineralogical Society of America Monograph,* 799 pp.

Spear, F., Kohn, M. & Cheney, J. 1999: *P-T* paths from anatectic pelites. *Contributions to Mineralogy and Petrology 134,* 17–32.

Stephens, M. B., Gustavson, M., Ramberg, I. B. & Zachrisson, E. 1985: The Caledonides of central-north Scandinavia – a tectonostratigraphic overview. *In* Gee, D. G. & Sturt, B. A. (eds.) *The Caledonide Orogen – Scandinavia and Related Areas.* John Wiley & Sons Ltd., 135–162.

Thorsnes, T. & Løseth, H. 1991: Tectonostratigraphy in the Velfjord-Tosen region, southwestern part of the Helgeland Nappe Complex, Central Norwegian Caledonides. *Norges geologiske undersøkelse Bulletin 421,* 1–18.

Trønnes, R. G. 1994: Marmorforekomster i Midt-Norge: Geologi, isotopgeokjemi og industrimineralpotensiale. *Norges geologiske undersøkelse Rapport 94.042,* 21 pp.

Watson, E. B. 1979: Zircon saturation in felsic liquids: experimental results and applications to trace element geochemistry. *Contributions to Mineralogy and Petrology 70,* 407–419.

Watson, E. B. 1996: Dissolution, growth and survival of zircons during crustal fusion: kinetic principles, geological models and implications for isotopic inheritance. *Transactions of the Royal Society of Edinburgh: Earth Sciences 87,* 43–56.

Watson, E. B. & Harrison, T. M. 1983: Zircon saturation revisited: temperature and composition effects in a variety of crustal magma types. *Earth and Planetary Science Letters 64,* 295–304.

Watson, E. B. & Harrison, T. M. 1984: Accessory minerals and the geochemical evolution of crustal magmatic systems: A summary and prospectus of experimental approaches. *Physics of Earth and Planetary Interiors 35,* 19–30.

Zen, E.-A. & Hammarstrom, J. M. 1984: Magmatic epidote and its petrologic significance. *Geology 12,* 515–518.